International Journal of Radiation Oncology biology • physics

www.redjournal.org

Biology Contribution

# Synchrotron Microbeam Radiation Therapy as a New Approach for the Treatment of Radioresistant Melanoma: Potential Underlying Mechanisms

**Marine Potez, PhD,* Cristian Fernandez-Palomo, PhD,* Audrey Bouchet, PhD,*,† Verdiana Trappetti, MSc,* Mattia Donzelli, PhD,‡,§ Michael Krisch, PhD,‡ Jean Laissue, MD,* Vladislav Volarevic, PhD,‖ and Valentin Djonov, MD***

**Institute of Anatomy, University of Bern, Bern, Switzerland; †Synchrotron Radiation for Biomedicine, INSERM UA7, 71 rue des Martyrs, 38000 Grenoble, France; ‡Biomedical Beamline ID17, European Synchrotron Radiation Facility, Grenoble, France; §Joint Department of Physics, The Institute of Cancer Research and the Royal Marsden Hospital, London, United Kingdom; and ‖Department of Microbiology and Immunology, Center for Molecular Medicine and Stem Cell Research, Faculty of Medical Sciences, University of Kragujevac, Serbia*

Received Apr 1, 2019. Accepted for publication Aug 18, 2019.

**Summary**

Synchrotron microbeam radiation therapy (MRT) is a unique treatment that spatially distributes the x-ray beam into several microbeams of very high dose. MRT significantly delays tumor regrowth compared with uniform radiation therapy. The underlying mechanisms include tumor vascular disruption, senescence, and inflammatory and antitumor

**Purpose:** Synchrotron microbeam radiation therapy (MRT) is a method that spatially distributes the x-ray beam into several microbeams of very high dose (peak dose), regularly separated by low-dose intervals (valley dose). MRT selectively spares normal tissues, relative to conventional (uniform broad beam [BB]) radiation therapy.

**Methods and Materials:** To evaluate the effect of MRT on radioresistant melanoma, B16-F10 murine melanomas were implanted into mice ears. Tumors were either treated with MRT (407.6 Gy peak; 6.2 Gy valley dose) or uniform BB irradiation (6.2 Gy).

**Results:** MRT induced significantly longer tumor regrowth delay than did BB irradiation. A significant 24% reduction in blood vessel perfusion was observed 5 days after MRT, and the cell proliferation index was significantly lower in melanomas treated by MRT compared with BB. MRT provoked a greater induction of senescence in melanoma cells. Bio-Plex analyses revealed enhanced concentration of monocyte-attracting chemokines in the MRT group: MCP-1 at D5, MIP-1α, MIP-1β, IL12p40,

Corresponding author: Valentin Djonov, MD; E-mail: valentin.djonov@ana.unibe.ch

The present work was supported by the Swiss National Foundation (31003A_176038), Swiss Cancer Research (KFS-4281-08-2017), and Bernische Krebsliga (grant number 190).

Disclosures: none.

Supplementary material for this article can be found at https://doi.org/10.1016/j.ijrobp.2019.08.027.

*Acknowledgments*—The authors have dedicated this work to their colleague Elke Bräuer-Krisch, who sadly passed away on September 10, 2018. Elke was a respected, essential, and enthusiastic promoter of microbeam radiation therapy and a key partner in preparing the way toward the clinical application of microbeam radiation therapy. The authors also thank Prof. John W. Hopewell for critical reading of the manuscript.

Int J Radiation Oncol Biol Phys, Vol. 105, No. 5, pp. 1126–1136, 2019



https://doi.org/10.1016/j.ijrobp.2019.08.027

immune responses. MRT could be considered a new and promising therapeutic approach in the treatment of radioresistant melanoma.

and RANTES at D9. This was associated with leukocytic infiltration at D9 after MRT, attributed mainly to CD8 T cells, natural killer cells, and macrophages.

**Conclusions:** In light of its potential to disrupt blood vessels that promote infiltration of the tumor by immune cells and its induction of senescence, MRT could be a new therapeutic approach for radioresistant melanoma. 

## Introduction

Microbeam radiation therapy (MRT) is an alternative radiation therapy technique based on the spatial fractionation and distribution of the synchrotron x-ray beam into many microbeams. This configuration allows the deposition of very high peak doses in the microbeam paths, whereas the tissue located between the microbeams receives only 1% to 10% of the peak dose (valley dose).[1,2] Although the microbeam peaks cover only ∼12% to 25% of the irradiated area, the therapeutic efficiency has proven to be high in small laboratory animals bearing tumors of different types (EMT6 carcinoma,[3] SCCVII carcinoma,[4] and 9L gliosarcoma[5-7]). Moreover, normal tissues showed only limited damage in response to the very high peak doses deposited by microbeams.[8,9] The mechanisms and the chronology underlying the MRT-induced antitumor response are not well understood, but studies have reported preferential effects of MRT on immature over mature blood vessels,[10-12] a differential gene expression between MRT and uniform broad beam (BB) irradiation regarding cell death,[13-15] and effects on immune and inflammatory responses.[16-18]

To gain a better understanding of the mechanisms involved in the efficiency of MRT, a melanoma model was selected. Malignant melanoma is among the most aggressive cancers, radioresistant and often producing metastases.[19] Conventional radiation therapy, stereotactic radiosurgery, and spatially distributed (sieve) radiation therapy have been used, mainly as a palliative strategy for patients with locally recurrent or metastatic melanoma; this treatment is efficient in 40% to 50% of patients.[20] Radiation therapy can be prescribed as a first-line treatment in cases where surgery would result in severe disfigurement or medical comorbidities (ie, mainly for cutaneous, uveal, or mucosal melanoma).[20]

In this study, the antitumor efficacy of MRT on a radioresistant melanoma was evaluated and compared with uniform irradiation (BB). The applied BB dose was equivalent to the MRT valley dose deposited in the tumors. The significantly better tumor control achieved by MRT has been related to (1) vascular disruption, (2) cell turnover, and (3) enhanced production of monocyte-attracting chemokines in the tumor microenvironment, followed by an increased number of tumor-infiltrating leukocytes.

## Methods and Materials

### Animals

All experiments were approved by the veterinary office of the Canton of Bern (BE61/15), and by the ESRF Internal Evaluation Committee for Animal Welfare and Rights (14_ethax22). Eight-week-old female C57BL/6J mice (Charles River Laboratories) were anesthetized by an intraperitoneal injection of a mixture of fentanyl 0.05 mg/kg body weight (b.w.), midazolam 5 mg/kg b.w., medetomidin 0.5 mg/kg b.w., and 5.6 mL/kg b.w. of sodium chloride 0.9%. All mice were humanely killed by pentobarbital intraperitoneal injection (50 mg/kg b.w.) at the end of the study (ie, 35 days after tumor implantation), or earlier, for sample collection or if a tumor ulcerated.

### Induction of melanoma

Radioresistant B16-F10 melanoma cells,[21,22] mixed with a fibrinogen matrix, were locally implanted in the ears of C57BL/6J mice, as described previously.[23] Briefly, under anesthesia, 3 skin incisions were made in a square shape on the ventral surface of the ear. The skin was peeled back, and a smaller square of the underlying cartilage was removed and replaced by a "tumor clot" (120000 B16-F10 cells in 4 μL volume, 3 μL of fibrinogen [3 mg/mL, Sigma], and 3 μL of thrombin [18 U/mL with 2mM $CaCl_2$; Sigma]). The skin flap was finally repositioned over the clot, and the incisions were closed with surgical glue (Histoacryl, Braun).

### Dosimetry and irradiation

The spatial configuration of the irradiation (microbeams or uniform BB) was verified using radiochromic film (Gafchromic, HD-810) placed behind the irradiated mouse ear. The doses were estimated with a Monte Carlo simulation based on the Geant4 toolkit[24] with microbeam fields and uniform BB fields. The ear of the mouse was modeled as a 0.3 mm thick disk with a 10 mm diameter, composed of

water. The tumor was inserted, represented as a 1.78 mm diameter water sphere in the center of the disk. By comparison with a Monte Carlo simulation performed in a large homogeneous water phantom, output factors relative to reference dosimetry conditions[25] were identified. According to the calculation, the peak to valley dose ratio inside the tumor was 65.7.

The irradiations were performed on the ID17 biomedical beamline at the European Synchrotron Radiation Facility (ESRF, France) with synchrotron x-rays, as described previously.[9] Ten to 11 days after tumor implantation, mice were separated into MRT-treated, uniform BB-treated, and nonirradiated (control) groups. The mice were placed vertically, with the head retained by a tooth bar and muzzle clamp. Each ear was fastened by adhesive tape at the extremity of the ear to avoid any x-ray scattering. For the BB group, a homogeneous beam 7.5 mm wide and 15 mm high delivered a dose of 6.2 Gy to the tumor (20.74 Gy/s/mA). For the MRT group, the irradiation field (7.5 mm wide and 15 mm high) was covered by 37 vertical quasiparallel microbeams (50 μm wide) produced by an ESRF Multislit Collimator (50 μm slits, spaced 200 μm apart center to center). The peak dose deposited in the tumor was 407.6 Gy, and the valley dose was 6.2 Gy (68.78 Gy/s/mA). Mice in the control group were sham irradiated.

## Tumor response

The tumor growth curves, from 2 independent experiments, were created by measuring the size of the tumors with a digital caliper. The tumor volume (V, $mm^3$; Fig. 1) was determined using the formula

$$V = \frac{4}{3}\pi \times \frac{a}{2} \times \frac{b}{2} \times \frac{c}{2}$$

where a, b, and c are, respectively, the length, width, and thickness of the tumor. The tumors were measured 3 days before irradiation, on the day of irradiation, and then daily for 20 days. A total of 101 tumors were used to evaluate the tumor regrowth delay: 47 for MRT, 28 for BB, and 26 in the control group.

## Histologic analyses

### Immunofluorescence

At autopsy, all tumors were frozen in isopentane and stored at −80°C. A total of 75 tumors distributed in 5 to 7 tumors (1 tumor per mouse) per group and per time point (day [D] −1, 2, 5, 9, and 12) were processed for histology. Immunostaining of endothelial cells (anti-CD31, BD Pharminogen), proliferating cells (anti-Ki67, Thermo-Fisher Scientific), T cells (anti-CD4, Abcam; anti-CD8, Abcam), natural killer (NK) cells (anti-CD161/NK1.1, Novus), and macrophages (anti-CD68, Biorad) were performed as detailed in Materials E1 (available online at https://doi.org/10.1016/j.ijrobp.2019.08.027).

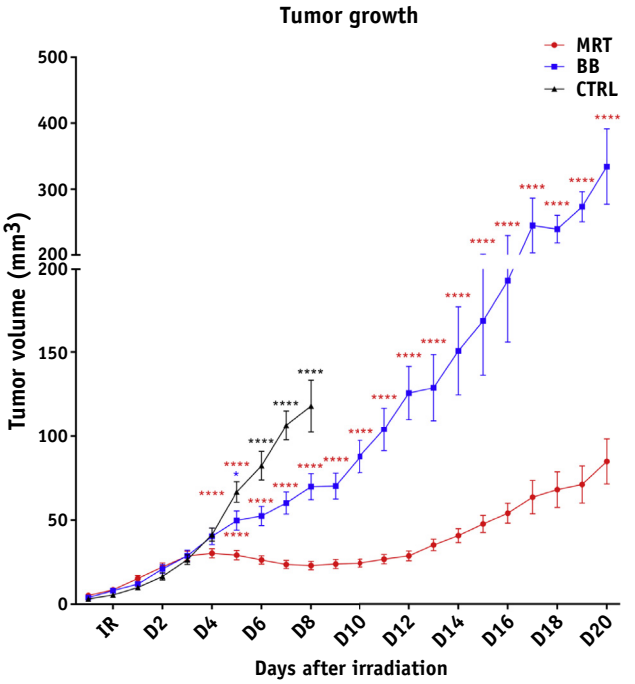


**Fig. 1.** Effect of irradiations on melanoma regrowth delay. Volume curves of tumors irradiated by microbeam radiation therapy (MRT) (red), by broad beam (BB) (blue), or nonirradiated (CTRL) (black). Red stars: significant difference between MRT and BB or CTRL groups. Blue star: significant difference between BB and CTRL groups. Black stars: significant difference among the CTRL, MRT, and BB groups. Mean ± standard error of the mean; $*P < .05$; $****P < .0001$. (A color version of this figure is available at https://doi.org/10.1016/j.ijrobp.2019.08.027).

To evaluate tumor perfusion, mice were injected with FITC-albumin (20 mg/mL, 2 mg/kg; Sigma) via the tail vein; after a circulation period of 1 hour, the tumors were processed as described in Materials E1 (available online at https://doi.org/10.1016/j.ijrobp.2019.08.027). Tumor slices cut from 97 tumors (6-8 tumors/group/time point, 1 tumor per mouse) were stained with anti-CD31 (BD Pharminogen) as primary antibody and Alexa Fluor 594 (Molecular Probes) as secondary antibody. This stained endothelial cells red, and perfused vessels appeared green (Fig. 2D).

### Image acquisition and analysis

Fluorescent CD31 immunostained images were acquired using a Leica M205FA microscope and Leica software LAS X (objective ×10; field of view [FOV]: 1.2614 $mm^2$). An in-house macro, incorporated into ImageJ software (https://imagej.nih.gov/ij/), was used to draw the shape of the CD31-positive vessels, and these images were merged with the associated FITC-albumin images (Fig. 2D). The number of vessels (CD31+) and perfused vessels (CD31+ and FITC-albumin+) were reported per FOV.

For the analysis of Ki67, CD4, CD8, CD161/NK1.1, and CD68 expression, 4 images per tumor (2 central and 2 peripheral), were obtained using a Zeiss Axioplan2 microscope

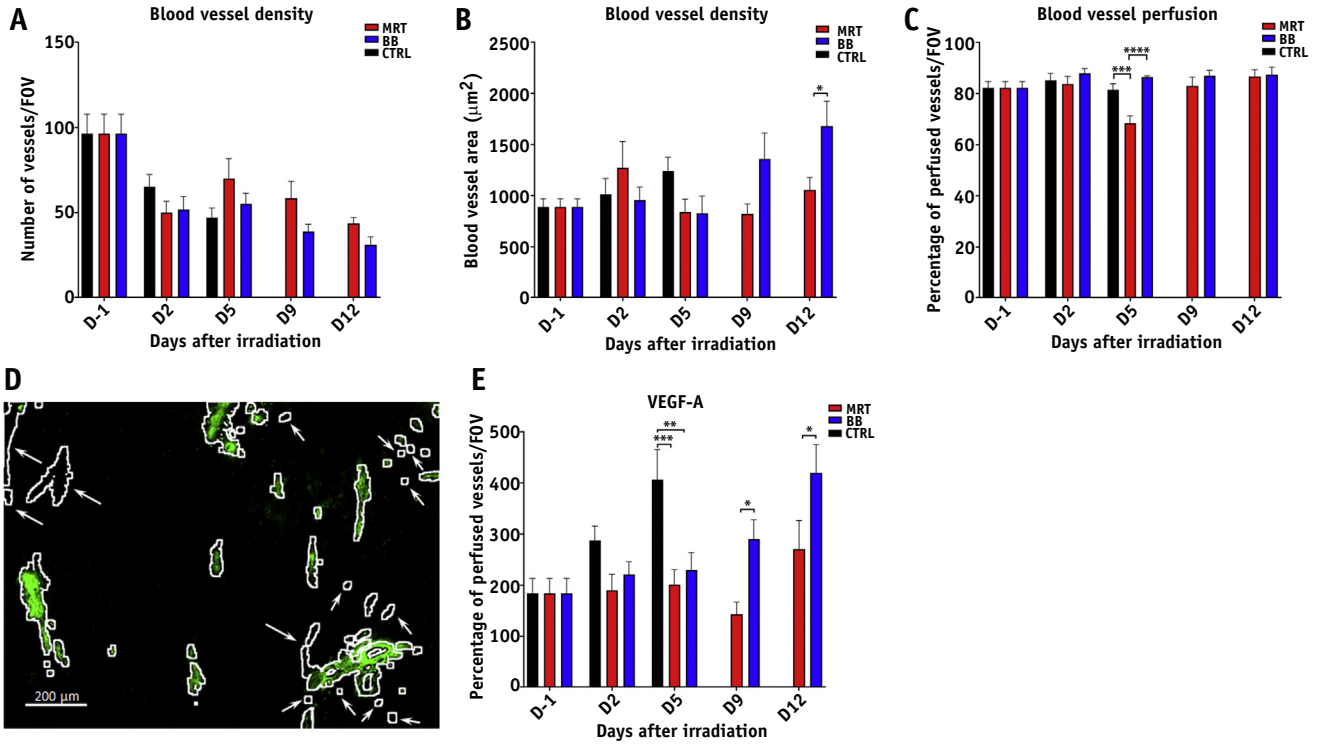


**Fig. 2.** Effects of irradiations on melanoma blood vessels. (A) Intratumoral microvascular density has been estimated by the number of CD31 positive vessels per field of view (FOV). (B) Area of blood vessels per FOV, represented by the total surface ($\mu m^2$) occupied by blood vessels. (C) Fractional percentage of perfused blood vessels per FOV. (D) Illustration of the methodology. White contours: CD31+. Green staining: FITC-albumin+. Arrows: nonperfused vessels (CD31+ and FITC-albumin−). (E) Concentration of VEGF-α in tumors after microbeam radiation therapy (red), broad beam (blue), or sham-irradiation (black). Mean ± standard error of the mean; $*P < .05$; $**P < .01$; $***P < .001$; $****P < .0001$. (A color version of this figure is available at https://doi.org/10.1016/j.ijrobp.2019.08.027.).

with Visiview software (objective ×20; FOV: 0.466 $mm^2$). Proliferating Ki67-positive cells were counted among a random selection of 100 nuclei stained with DAPI. T cells, NK cells, and macrophages were evaluated by a scoring system of 1 to 4, adapted from,[9] representative of the approximate number of immunostained cells (CD4 and CD8: 1, <5%; 2, 5%-12%; 3, 13%-20%; 4, >20%; NK cells and macrophages: 1, <10%; 2, 10%-20%; 3, 21%-40%; 4, >40%) (Fig. E1; available online at https://doi.org/10.1016/j.ijrobp.2019.08.027).

### Senescence-associated β-galactosidase staining and image analysis

Eighty-two tumors were collected, and frozen sections from 5 to 11 tumors/group/time point (1 tumor per mouse) were stained with senescence-associated β-galactosidase (SA β-Gal, Sigma) (Materials E1; available online at https://doi.org/10.1016/j.ijrobp.2019.08.027). Four images per tumor (objective ×10; FOV, 1.45 $mm^2$) were captured with a Zeiss Imager M2 Light microscope and Cell D software. Senescent cells were evaluated by a score of 1 to 4, to represent the approximate tumor area occupied by immunostained cells (0, 0%; 1, 0%-5%; 2, 5%-10%; 3, 10%-15%; 4, >15%) (Fig. E2; available online at https://doi.org/10.1016/j.ijrobp.2019.08.027).

### Enzyme-linked immunosorbent assay and Bio-Plex analyses

Proteins from 109 tumors (6-12 frozen pieces of tumors/group/time point, 1 tumor per mouse) were extracted (Material E1; available online at https://doi.org/10.1016/j.ijrobp.2019.08.027). Tumor tissue homogenates were tested for a panel of 23 cytokines (Bio-Plex Pro Mouse Assay, Bio-rad) and VEGF-α (ELISA kit, LSBio), according to the manufacturers' instructions. Dilution and analyses are detailed in Material E1 (available online at https://doi.org/10.1016/j.ijrobp.2019.08.027). All cytokines without a significant difference between MRT and BB groups are presented in Figure E3 (available online at https://doi.org/10.1016/j.ijrobp.2019.08.027).

### Statistical analysis

GraphPad Prism (GraphPad Software, San-Diego, CA) 2-way analysis of variance with Sidak posttest program was used. Values were considered significantly different when $P < .05$, and results are presented as means ± standard error of the mean.

## Results

### Dosimetry

Reference dosimetry in BB configuration was performed using a PinPoint PTW 31014 ionization chamber (PTW, Freiburg, Germany). The PinPoint chamber was calibrated for absorbed dose to water in $^{60}$Co and TH200 beam qualities. The detector was biased at 400 V and read out using a PTW Unidos Webline electrometer. Correction factors for ion recombination[26] and temperature and pressure[27] were determined and applied to the measurements. Monte Carlo simulations based on the Geant4 toolkit then were used to convert the reference dose to the dose within the microbeam field.[24]

### Tumor regrowth delay after MRT and BB irradiation

MRT- and BB-treated mice showed significantly impeded tumor growth from D5 compared with nonirradiated tumors (control) (Fig. 1, $P < .005$). Although almost exponential growth was seen in the BB-irradiated tumors until the end of the examination, MRT-treated tumors reached a volume of 30.4 ± 2.7 mm$^3$ on D4 before the volume decreased slightly over the next 4 days. MRT-treated tumors regrew during the next 12 days. The doubling times of tumor volume were 2.1 days in the control group, 3.7 days in the BB, and 6 days in the MRT groups.

### MRT disrupts tumor vascular perfusion

The immunostaining of CD31-positive endothelial cells (Fig. E4; available online at https://doi.org/10.1016/j.ijrobp.2019.08.027) revealed that the number of intratumoral blood vessels did not differ significantly among the 3 groups (Fig. 2A). A tendential increase in the number of blood vessels was suggested in the MRT-treated group on D5 (69.7 ± 12 vessels per FOV), but this was not a significant difference ($P > .05$) from the values of 55 ± 6.3 and 47 ± 5.7 vessels per FOV for the BB and control groups, respectively. The blood vessel area did not differ among the control, MRT, and BB groups in the first week after irradiation (Fig. 2B, $P > .05$). From D9, the BB group seemed to have larger blood vessels (1355.6 ± 255.1 mm$^2$) compared with the MRT group (819.3 ± 97.3 mm$^2$). This difference was significant at D12 (1675.4 ± 245 mm$^2$ for BB vs 1052.5 ± 123.7 mm$^2$ for MRT, $P < .05$). Figures 2C and 2D show the quantification of the blood vessel perfusion, and the fraction of perfused blood vessels in all groups over all time points was in a range of 80% to 90%. A notable exception was observed by D5 in the MRT group, where the percentage of perfused vessels was significantly lower (68.5% ± 2.3%) compared with the BB (86.3% ± 0.6%, $P < .01$) and the control groups (81.5% ± 2.3%, $P < .001$; Fig. 2C). Figure 2D shows a representative example of perfused vessels (green staining surrounded by white outline) and nonperfused vessels (with outline indicated by arrows).

Evaluation of VEGF-α concentration showed a significant increase in control tumors (406 ± 59 pg/mL of protein) compared with irradiated tumors (MRT, 201.4 ± 29 pg/mL of protein, $P < .001$; BB, 228.8 ± 34.7 pg/mL of protein, $P < .01$). On D9, a significant decrease in VEGF-α concentration was shown in the MRT group (142.6 ± 24.1 pg/mL of protein) compared with the BB group (289.9 ± 37.9 pg/mL of protein; $P < .05$; Fig. 2E).

### MRT reduces proliferation and induces senescence of tumor cells

Irradiated tumors showed a decrease in the cell proliferation index (Ki-67), compared with the control tumors, starting from D2 in the MRT group (69.8% ± 3.6% vs 55.8% ± 2.3%, respectively, $P < .05$) and from D5 for the BB group (70.8% ± 1.9% vs 51.9% ± 2.3%, respectively, $P < .01$) (Fig. 3A). The MRT group showed a significantly lower tumor cell proliferation rate on D5 compared with the BB group (23.2% ± 5.2% vs 51.9% ± 2.3%, respectively; $P < .0001$), with a maximum divergence on D9 (14.5% ± 3.6% vs 70.9% ± 4.8%, respectively; $P < .0001$). Figure 3B shows a notable increase of SA-β-gal (senescence marker) in MRT-irradiated tumors. The senescence index was significantly higher after MRT from D2 to D9 compared with control ($P < .01$ and $P < .0001$ at D2 and D5, respectively) and BB-treated tumors ($P < .05$, $P < .0001$, and $P < .001$ at D2, D5, and D9, respectively).

### MRT significantly enhanced the production of monocyte-attracting cytokines in the tumor microenvironment

MRT significantly enhanced the production of monocyte-attracting cytokines in the tumor microenvironment. The concentration of chemokines monocyte chemoattractant protein (MCP)-1, macrophage inflammatory protein (MIP)-1α, MIP-1β, regulated upon activation normal T cell expressed and secreted (RANTES), and interleukin (IL) 12p40, which are involved in recruitment and migration of circulating monocytes in the tumor tissue,[28,29] were significantly higher in the MRT group compared with BB and control groups (Fig. 4). The concentration of MCP-1 was higher in MRT-treated tumors at D5 (2066.1 ± 188.1 pg/mL of protein) compared with the BB-treated (1406.6 ± 171.4 pg/mL of protein, $P < .05$) and the control tumors (705.3 ± 132.3 pg/mL of protein; $P < .0001$) (Fig. 4A). At D9, a significantly higher concentration of MIP-1a (2.56-fold, $P < .05$, Fig. 4B), MIP-1b (2.29-fold, $P < .05$, Fig. 4C), IL12p40 (2.66-fold, $P < .01$, Fig. 4D), and RANTES (2.06-fold, $P < .05$, Fig. 4E) was observed after MRT compared with BB irradiation.

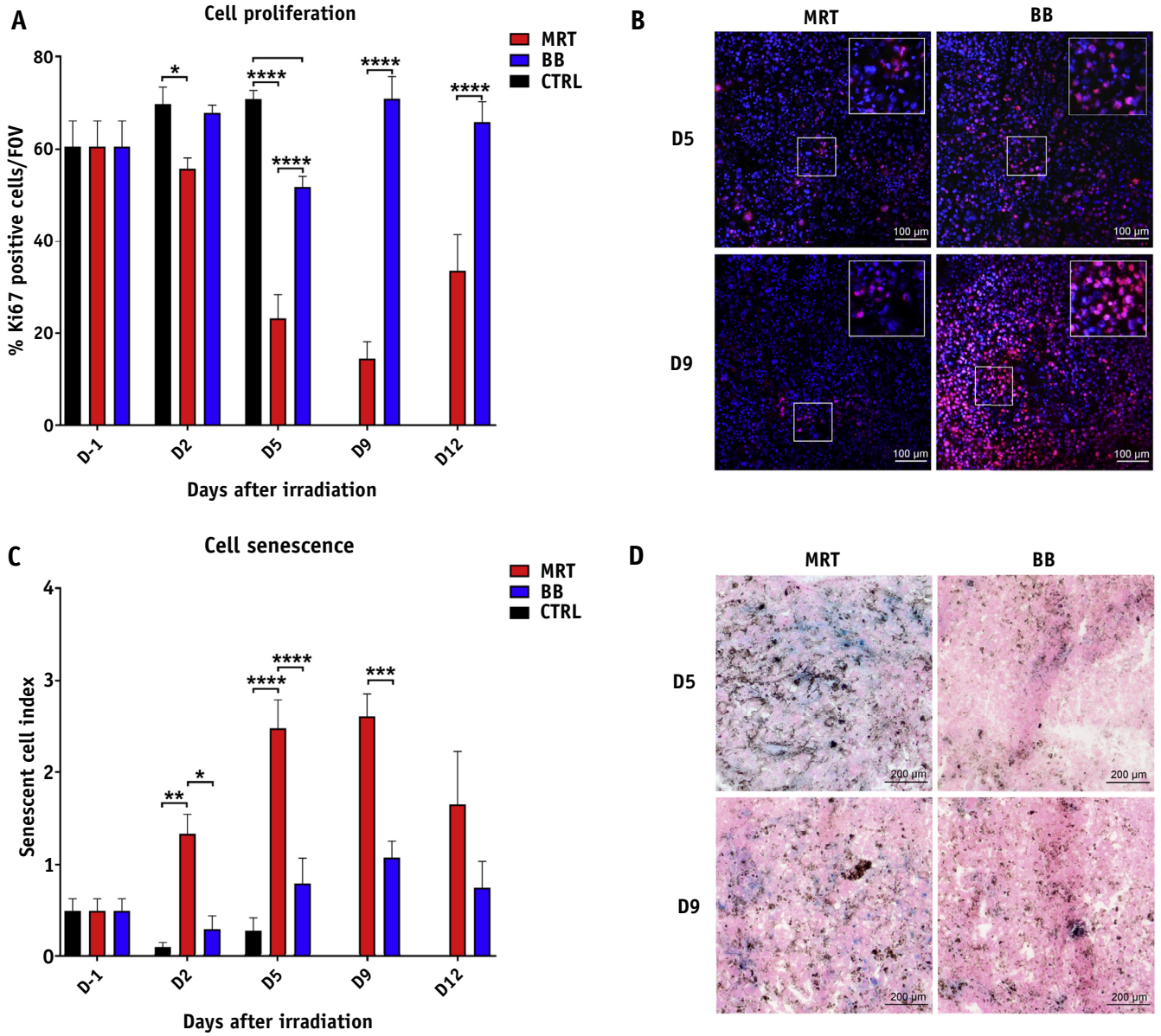


**Fig. 3.** Effects of irradiations on melanoma tumor cells turnover. (A) Percentage of Ki67+ cells among 100 DAPI+ nuclei per field of view. (B) Representative images of microbeam radiation therapy (MRT) (left column) and broad beam (BB) (right column) irradiated tumors immunostained by KI67 (red) and DAPI (blue) at D5 and D9. Magnification ×20; scale bars 100 µm. Right upper corner square: zoom in from the indicated areas. (C) Estimation of senescent cell density per field of view in MRT (red), BB (blue), and control (black) tumors. (D) Illustrations of MRT (left column) and BB (right column) irradiated tumors stained by SA-β-galactosidase (blue coloration). The dark spots correspond to melanin pigment. Magnification ×10; scale bars 200 µm. Mean ± standard error of the mean; $*P < .05$; $**P < .01$; $***P < .001$; $****P < .0001$. (A color version of this figure is available at https://doi.org/10.1016/j.ijrobp.2019.08.027.).

In MRT-treated tumors, a notably higher presence of immune cells was seen from D5 to D12 compared with the other groups (Fig. 5). Immunostaining revealed that MRT promoted peritumoral and intratumoral infiltration of macrophages, CD4+ and CD8+ T lymphocytes, and NK cells (Fig. 5). A notably higher presence of these immune cells was noted at D5 (Fig. 5Bii) and D9 (Fig. 5Biii) in MRT-treated tumors compared with nonirradiated or BB-treated tumors.

## Discussion

This study is the first to demonstrate the therapeutic potential of MRT to treat radioresistant melanoma. MRT transiently suppressed growth and progression of the B16-F10 mouse melanoma by acting as a tumor vascular disrupting and immunomostimulatory agent. MRT induced tumor senescence and elicited tumor inflammatory and

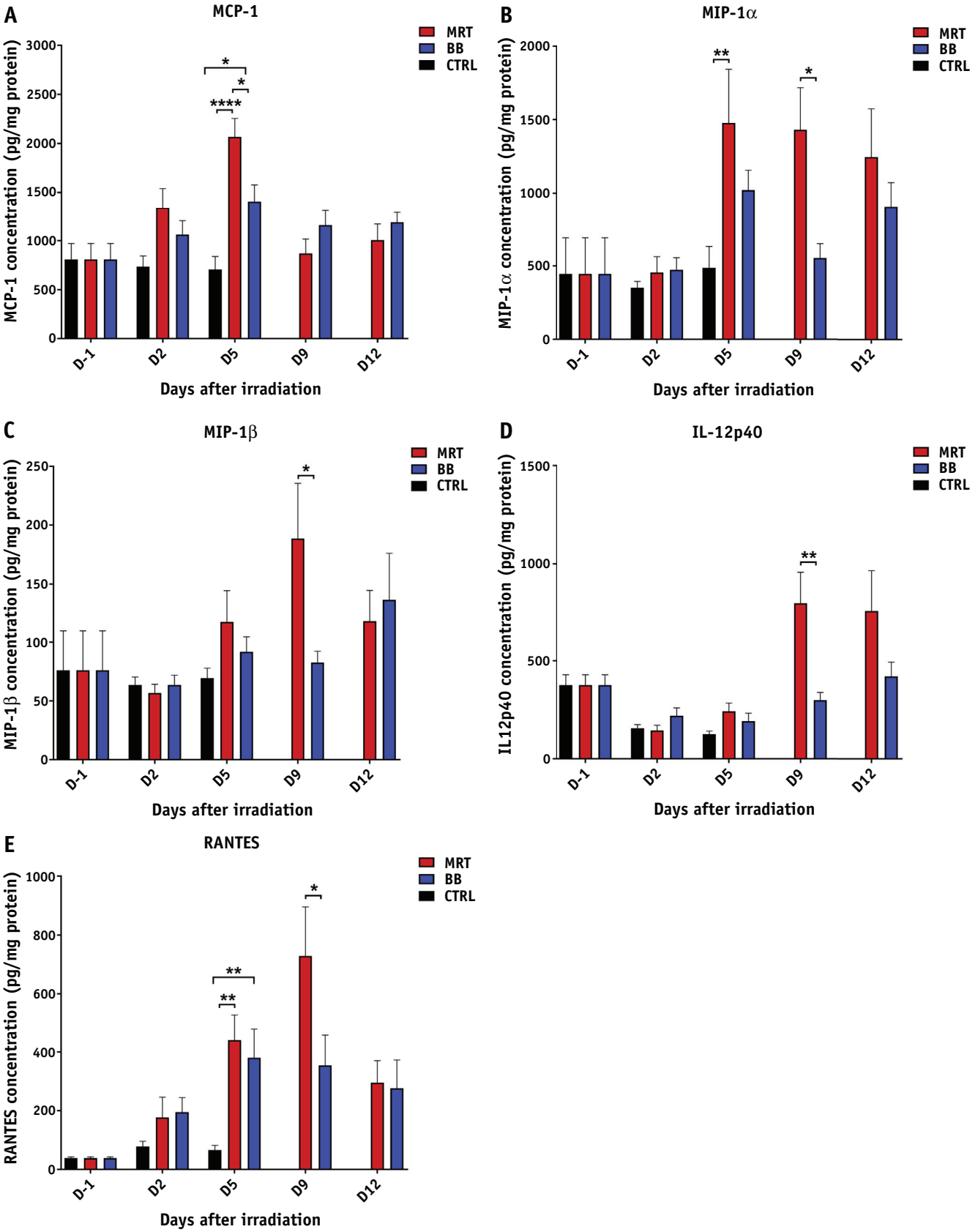


**Fig. 4.** Effects of irradiations on melanoma microenvironment. Cytokine expression in B16-F10 tumors exposed to microbeam radiation therapy (red), broad beam (blue), or nonirradiated (black). Mean ± standard error of the mean; *$P <$ .05; **$P <$ .01; ****$P <$ .0001. (A color version of this figure is available at https://doi.org/10.1016/j.ijrobp.2019.08.027.).

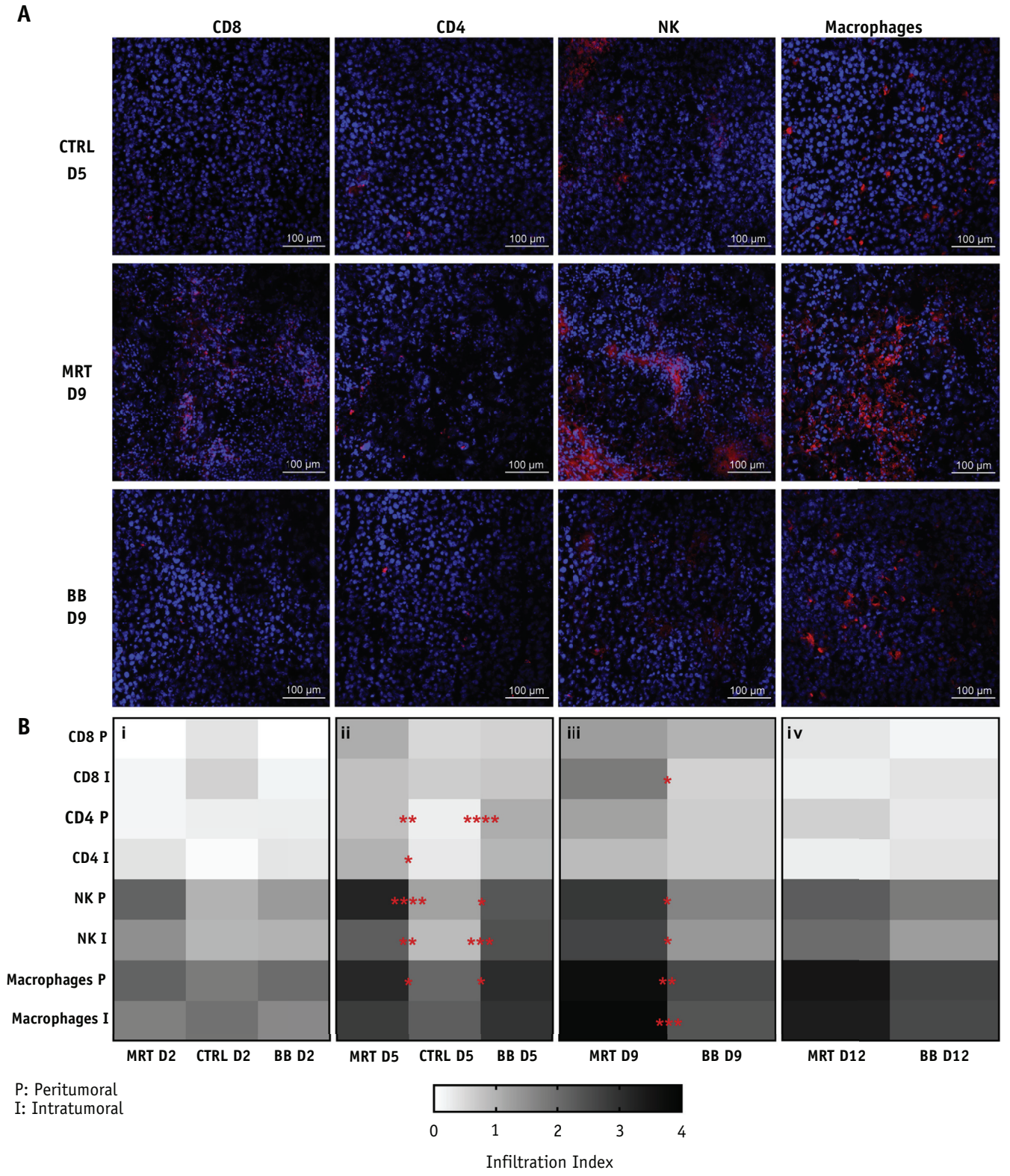


**Fig. 5.** Effects of irradiations on melanoma infiltration by immune cells. (A) Representative images of immunostained tumor cells (blue = DAPI), immune cells (CD8 [red], CD4 [red], NK [red] and macrophages [red]) in the control group at D5 (no survivors at D9) and in the microbeam radiation therapy and broad beam groups at D9. Magnification, ×20. Scale bars, 100 µm. (B) Heat map showing the infiltration index of CD8 and CD4 T cells, natural killer cells, and macrophages in peritumoral or intratumoral area, per group at D2 (i), D5 (ii), D9 (iii), and D12 (iv) after irradiation. The color code, from white to black, represents the scoring system from 0 to 4. Red stars between 2 columns: significant changes between groups. Mean ± standard error of the mean; $*P < .05$; $**P < .01$; $***P < .001$; $****P < .0001$. (A color version of this figure is available at https://doi.org/10.1016/j.ijrobp.2019.08.027.).

immune response by promoting the production of monocyte-attracting chemokines in the tumor microenvironment.

The relevant radiobiological dose measured during MRT is a matter of ongoing research. Early studies in MRT used the peak dose to compare the biological results[30,31] because the peak dose is the most easily accessible quantity. However, more recent results show that the valley dose is most likely the deciding factor in regard to biological effects.[17,32] This view has been supported by other authors who demonstrated that (1) the valley dose of MRT is the most relevant parameter for acute toxicity[33] and (2) the integrated dose is not a useful indicator of the biological equivalence of MRT and BB.[34]

MRT significantly attenuated melanoma growth during the 20 days of follow-up, whereas BB irradiation did not manage to temporarily stop melanoma growth and progression. Our results are in line with studies previously published[17,35] showing that MRT had superior efficacy in slowing brain tumor growth in comparison to BB. As shown recently, a unidirectional microbeam irradiation (400 Gy and 17.4 Gy as peak and valley doses, respectively) induced better tumor control and survival than BB irradiation (17.9 Gy) in glioma-bearing rats.[17] It was suggested that part of the better tumor control achieved by MRT could be attributed to the immediate cell death caused by the high dose delivered by the microbeams.[14,17] However, only one-quarter of the total targeted tissue was exposed to the high dose in microbeams, whereas three-quarters was exposed to the low valley dose. Therefore, this discrete dose distribution achieved significant tumor growth delay while sparing the normal tissue. The latter is particularly important when the tumors are localized in the vicinity of or inside a radiosensitive organ.

MRT altered blood vessel integrity and significantly reduced blood perfusion in irradiated tumors (Fig. 2A), indicating its potential to act as a vascular disruption agent in radio-oncology. Studies on chick chorioallantoic membrane and zebrafish caudal fin regeneration models, showing 2 types of immature vessels, demonstrated that MRT induced notable morphologic and functional damage[10] and severely impaired vascular perfusion[12] of immature blood vessels. Two main mechanisms were identified: (1) direct disruption of immature capillaries along the beam path, which caused endothelial cell detachment and consequent folding into the lumen; and (2) local adhesion of blood cells at the site of vascular damage. Importantly, both events interrupted vessel perfusion and efficiently prevented blood supply even in the first hours after irradiation. Accordingly, we assume that MRT-based attenuation of melanoma growth and progression was a consequence of endothelial cell disruption and inflammatory cell infiltration of irradiated tumors. Moreover, MRT significantly downregulated the production of VEGF-α (Fig. 2C), a major proangiogenic cytokine responsible for tumor expansion and metastasis.[36,37] Therefore, by suppressing VEGF-α–dependent neoangiogenesis, MRT transiently suppressed melanoma growth and progression (Fig. 1).

According to our results, the significant tumor control after MRT seems to be linked to the induction of senescence, inflammation, and antitumor immune cell infiltration. In this study, however, we did not analyze effects of MRT on the induction of apoptosis because other authors have found only few apoptotic cells after MRT.[14,15] A significant decrease in the total number of proliferating cells was observed in MRT-irradiated tumors from D2 to D12 (Fig. 3A), suggesting that more MRT-irradiated melanoma cells were either in the G0 phase or dying rather than in the cell cycle. This event was probably a result of the MRT-induced senescence of melanoma cells that was detected from D2 to D9 (Fig. 3B). Senescence has already been postulated as an important mechanism of MRT-based antitumor effects against glioma cells.[15] The marker of senescence (β-galactosidase) employed in this study did not appear to display any changes that reflect the microbeam pattern; thus, we were not able to observe a differential effect between the high dose in the peak region and the low dose in the valley region. Senescent cells are no longer dividing but are still metabolically active. They overexpress or secrete proteins in the microenvironment that influence neighboring cells. This phenotype is known as the senescence-associated secretory phenotype (SASP) and might explain the absence of a differential effect between the peak and valley dose regions. The SASP includes the secretion of cytokines, growth factors, extracellular matrix protease, and immune cells attracting chemokines.[38-40] Here, we noted significantly elevated levels of MCP-1 and RANTES (Figs. 4), 2 cytokines expressed by senescent melanoma cells[39-41] in MRT-treated tumors. We hypothesize that MRT-induced senescence promoted the development of SASP in melanoma cells, causing the significant increase in the concentrations of monocyte-attracting chemokines MCP-1 and RANTES. These 2 chemokines are crucially involved in the recruitment of leukocytes in the inflamed and malignant tissues.[29] It is well known that irradiation attenuates tumor growth in an MCP-1 dependent manner by promoting homing of CCR2+ CCR5+ inflammatory monocytes.[29] In a manner similar to MCP-1 and RANTES, MIP-1α, MIP-1β, and IL-12p40 also promote migration and influx of inflammatory monocytes from the peripheral blood in the tumor tissue.[27,41,42] As shown in Figure 4, MRT significantly enhanced the release of these chemokines, resulting in a massive influx of macrophages, NK cells, and CD4+ and CD8+ T lymphocytes (Fig. 5). These immune cells could induce robust inflammatory and antitumor immune responses through the production of inflammatory cytokines (by macrophages and CD4+ T lymphocytes) or via direct cytotoxicity against melanoma cells (NK cell and CD8+ T lymphocytes), finally resulting in attenuated melanoma growth and progression.[43-45] Moreover, the intratumoral infiltration of these immune

cells appears to be a sign of a positive prognosis, including improved patient survival,[46-48] which means MRT has great potential.

Our study provided evidence that MRT has a greater effect on tumor control than does synchrotron BB irradiation. In addition, a recently published study demonstrated that the irradiated normal tissue surrounding the tumor is highly tolerant of MRT.[9] Different components of the tumor-bearing normal tissue, including cutis, subcutis, cartilage, blood, and lymphatic vessels, demonstrated no significant short- and long-term morphologic alteration by 400 Gy MRT. High normal tissue tolerance has been reported recently during experiments employing BB FLASH radiation therapy. The work of Favaudon et al in 2014 showed that by using ultra-high-dose-rate radiation therapy (>40 Gy/s; ie, FLASH), the normal tissue was spared; irradiation with the same dose at a lower dose rate (<0.03 Gy/s; conventional) caused important damage.[49] In comparison with conventional radiation therapy, FLASH radiation therapy did not induce lung fibrosis[49] or skin necrosis.[50] However, the beneficial effect on tumor control was the same for both treatments/[49] In contrast, MRT not only spares normal tissue but also exerts excellent tumor control. The differential effect between MRT and FLASH- radiation therapy is probably due to the spatial distribution of the dose. FLASH-radiation therapy applies a homogeneous BB dose with a high dose rate, whereas MRT uses an array of high peak and low valley dose with a high dose rate.

## Conclusions

This study demonstrated superior tumor control by MRT over BB irradiation of a mouse melanoma model, which is probably a result of the following events: (1) reduction in the tumor blood supply by vascular disruption and occlusion; (2) radiation-disrupted tumor endothelial cells serving as an entrance site for circulating inflammatory and immune cells; (3) MRT inducing a decrease in the proliferation index, associated with induced tumor senescence; (4) senescent cells seeming to secrete cytokines that initiate infiltration of different types of immune cells, such as T cells, NK cells, and macrophages, which are involved in the clearance of senescent cells and thus contribute to tumor control. Accordingly, MRT represents a promising candidate for new clinical trials, which should explore the clinical relevance of the MRT-based antitumor effects presented here.

## References


1. Bräuer-Krisch E, Serduc R, Siegbahn EA, et al. Effects of pulsed, spatially fractionated, microscopic synchrotron X-ray beams on normal and tumoral brain tissue. *Mutat Res* 2010;704:160-166.
2. Slatkin DN, Spanne P, Dilmanian FA, et al. Microbeam radiation therapy. *Med Phys* 1992;19:1395-1400.
3. Dilmanian FA, Morris GM, Zhong N, et al. Murine EMT-6 carcinoma: High therapeutic efficacy of microbeam radiation therapy. *Radiat Res* 2003;159:632-641.
4. Miura M, Blattmann H, Bräuer-Krisch E, et al. Radiosurgical palliation of aggressive murine SCCVII squamous cell carcinomas using synchrotron-generated X-ray microbeams. *Br J Radiol* 2006;79:71-75.
5. Laissue JA, Geiser G, Spanne PO, et al. Neuropathology of ablation of rat gliosarcomas and contiguous brain tissues using a microplanar beam of synchrotron-wiggler-generated X rays. *Int J Cancer* 1998;78:654-660.
6. Regnard P, Le Duc G, Bräuer-Krisch E, et al. Irradiation of intracerebral 9L gliosarcoma by a single array of microplanar x-ray beams from a synchrotron: Balance between curing and sparing. *Phys Med Biol* 2008;53:861-878.
7. Regnard P, Bräuer-Krisch E, Troprès I, et al. Enhancement of survival of 9L gliosarcoma bearing rats following intracerebral delivery of drugs in combination with microbeam radiation therapy. *Eur J Radiol* 2008;68:S151-S155.
8. Smyth LM, Senthi S, Crosbie JC, et al. The normal tissue effects of microbeam radiotherapy: What do we know, and what do we need to know to plan a human clinical trial? *Int J Radiat Biol* 2016;92:302-311.
9. Potez M, Bouchet A, Wagner J, et al. Effects of synchrotron x-ray micro-beam irradiation on normal mouse ear pinnae. *Int J Radiat Oncol Biol Phys* 2018;101:680-689.
10. Sabatasso S, Laissue JA, Hlushchuk R, et al. Microbeam radiation-induced tissue damage depends on the stage of vascular maturation. *Int J Radiat Oncol Biol Phys* 2011;80:1522-1532.
11. Bouchet A, Serduc R, Laissue JA, et al. Effects of microbeam radiation therapy on normal and tumoral blood vessels. *Phys Med* 2015;31:634-641.
12. Brönnimann D, Bouchet A, Schneider C, et al. Synchrotron microbeam irradiation induces neutrophil infiltration, thrombocyte attachment and selective vascular damage in vivo. *Sci Rep* 2016;6:33601.
13. Serduc R, Christen T, Laissue J, et al. Brain tumor vessel response to synchrotron microbeam radiation therapy: A short-term in vivo study. *Phys Med Biol* 2008;53:3609-3622.
14. Uyama A, Kondoh T, Nariyama N, et al. A narrow microbeam is more effective for tumor growth suppression than a wide microbeam: An in vivo study using implanted human glioma cells. *J Synchrotron Radiat* 2011;18:671-678.
15. Anderson DL, Mirzayans R, Andrais B, et al. Spatial and temporal distribution of γH2AX fluorescence in human cell cultures following synchrotron-generated X-ray microbeams: Lack of correlation between persistent γH2AX foci and apoptosis. *J Synchrotron Radiat* 2014;21:801-810.
16. Sprung CN, Yang Y, Forrester HB, et al. Genome-wide transcription responses to synchrotron microbeam radiotherapy. *Radiat Res* 2012;178:249-259.
17. Bouchet A, Bräuer-Krisch E, Prezado Y, et al. Better efficacy of synchrotron spatially microfractionated radiation therapy than uniform radiation therapy on glioma. *Int J Radiat Oncol Biol Phys* 2016;95:1485-1494.
18. Ibahim MJ, Yang Y, Crosbie JC, et al. Eosinophil-associated gene pathways but not eosinophil numbers are differentially regulated between synchrotron microbeam radiation treatment and synchrotron broad-beam treatment by 48 hours postirradiation. *Radiat Res* 2016;185:60-68.
19. Cummins DL, Cummins JM, Pantle H, et al. Cutaneous malignant melanoma. *Mayo Clin Proc* 2006;81:500-507.
20. Mahadevan A, Patel VL, Dagoglu N. Radiation therapy in the management of malignant melanoma. *Oncology (Williston Park)* 2015;29:743-751.
21. Korcum AF, Sanlioglu S, Aksu G, et al. Radiotherapy-induced decreases in substance P levels may potentiate melanoma growth. *Mol Med Rep* 2009;2:319-326.
22. Derer A, Spiljar M, Bäumler M, et al. Chemoradiation increases PD-L1 expression in certain melanoma and glioblastoma cells. *Front Immunol* 2016;7:610.
23. Potez M, Trappetti V, Bouchet A, et al. Characterization of a B16-F10 melanoma model locally implanted into the ear pinnae of C57BL/6 mice Mattei F, ed. *PLoS One* 2018;13:e0206693.
24. Allison J, Amako K, Apostolakis J, et al. Recent developments in Geant4. *Nucl Instrum Methods Phys Res A* 2016;835:186-225.

25. Fournier P, Crosbie JC, Cornelius I, et al. Absorbed dose-to-water protocol applied to synchrotron-generated x-rays at very high dose rates. *Phys Med Biol* 2016;61:N349-N361.
26. Fournier P, Cornelius I, Donzelli M, et al. X-Tream quality assurance in synchrotron x-ray microbeam radiation therapy. *J Synchrotron Radiat* 2016;23:1180-1190.
27. Absorbed Dose Determination in External Beam Radiotherapy: An International Code of Practice for Dosimetry Based Standards of Absorbed Dose to Water. Technical Report Series No. 398. Vienna, Austria; 2000.
28. Cooper AM, Khader SA. IL-12p40: An inherently agonistic cytokine. *Trends Immunol* 2007;28:33-38.
29. Connolly KA, Belt BA, Figueroa NM, et al. Increasing the efficacy of radiotherapy by modulating the CCR2/CCR5 chemokine axes. *Oncotarget* 2016;7:86522-86535.
30. Laissue JA, Blattmann H, Di Michiel M, et al. Weanling piglet cerebellum: A surrogate for tolerance to MRT (microbeam radiation therapy) in pediatric neuro-oncology. *Penetrating Radiat Syst Appl* 2001;4508:65-73.
31. Serduc R, Vérant P, Vial JC, et al. In vivo two-photon microscopy study of short-term effects of microbeam irradiation on normal mouse brain microvasculature. *Int J Radiat Oncol Biol Phys* 2006;64:1519-1527.
32. Serduc R, Bouchet A, Bräuer-Krisch E, et al. Synchrotron microbeam radiation therapy for rat brain tumor palliation - influence of the microbeam width at constant valley dose. *Phys Med Biol* 2009;54:6711-6724.
33. Smyth LML, Donoghue JF, Ventura JA, et al. Comparative toxicity of synchrotron and conventional radiation therapy based on total and partial body irradiation in a murine model. *Sci Rep* 2018;8:12044.
34. Ibahim MJ, Crosbie JC, Yang Y, et al. An evaluation of dose equivalence between synchrotron microbeam radiation therapy and conventional broadbeam radiation using clonogenic and cell impedance assays. *PLoS One* 2014;9:e100547.
35. Bouchet A, Potez M, Coquery N, et al. Permeability of brain tumor vessels induced by uniform or spatially micro-fractionated synchrotron radiation therapies. *Int J Radiat Oncol Biol Phys* 2017;98:1174-1182.
36. Jain RK. Antiangiogenesis strategies revisited: From starving tumors to alleviating hypoxia. *Cancer Cell* 2014;26:605-622.
37. Felcht M, Thomas M. Angiogenesis in malignant melanoma. *J Dtsch Dermatol Ges* 2015;13:125-136.
38. Roninson IB, Broude EV, Chang BD. If not apoptosis, then what? Treatment-induced senescence and mitotic catastrophe in tumor cells. *Drug Resist Updat* 2001;4:303-313.
39. Vicente R, Mausset-Bonnefont AL, Jorgensen C, et al. Cellular senescence impact on immune cell fate and function. *Aging Cell* 2016;15:400-406.
40. Coppé JP, Desprez PY, Krtolica A, et al. The senescence-associated secretory phenotype: The dark side of tumor suppression. *Annu Rev Pathol* 2010;5:99-118.
41. Payne AS, Cornelius LA. The role of chemokines in melanoma tumor growth and metastasis. *J Invest Dermatol* 2002;118:915-922.
42. Nakasone Y, Fujimoto M, Matsushita T, et al. Host-derived MCP-1 and MIP-1α regulate protective anti-tumor immunity to localized and metastatic B16 melanoma. *Am J Pathol* 2012;180:365-374.
43. Lee S, Margolin K. Tumor-infiltrating lymphocytes in melanoma. *Curr Oncol Rep* 2012;14:468-474.
44. Maccalli C, Scaramuzza S, Parmiani G. TNK cells (NKG2D+ CD8+ or CD4+ T lymphocytes) in the control of human tumors. *Cancer Immunol Immunother* 2009;58:801-808.
45. Wang H, Zhang L, Yang L, et al. Targeting macrophage anti-tumor activity to suppress melanoma progression. *Oncotarget* 2017;8:18486-18496.
46. Fridman WH, Galon J, Pagès F, et al. Prognostic and predictive impact of intra- and peritumoral immune infiltrates. *Cancer Res* 2011;71:5601-5605.
47. Baeten CI, Castermans K, Hillen HF, et al. Proliferating endothelial cells and leukocyte infiltration as prognostic markers in colorectal cancer. *Clin Gastroenterol Hepatol* 2006;4:1351-1357.
48. Baeten CI, Castermans K, Lammering G, et al. Effects of radiotherapy and chemotherapy on angiogenesis and leukocyte infiltration in rectal cancer. *Int J Radiat Oncol Biol Phys* 2006;66:1219-1227.
49. Favaudon V, Caplier L, Monceau V, et al. Ultrahigh dose-rate FLASH irradiation increases the differential response between normal and tumor tissue in mice. *Sci Transl Med* 2014;6:245ra93.
50. Vozenin MC, De Fornel P, Petersson K, et al. The advantage of FLASH radiotherapy confirmed in mini-pig and cat-cancer patients. *Clin Cancer Res* 2019;25:35-42.